Research Square

Preprints are preliminary reports that have not undergone peer review.
They should not be considered conclusive, used to inform clinical practice,
or referenced by the media as validated information.

# Numerical computation of Laplace operator spectra in starlike domains using the Vekua integral operator and singular value minimization

**Demidov Alexandre**
Lomonosov Moscow State University
**Lyakhov Dmitry**
dmlyakhov@gmail.com

RUDN University

**Method Article**

**Keywords:**

**Posted Date:** November 23rd, 2026

**DOI:** https://doi.org/10.21203/rs.3.rs-11700236/v1

**License:** This work is licensed under a Creative Commons Attribution 4.0 International License.
Read Full License

**Additional Declarations:** No competing interests reported.

# Numerical computation of Laplace operator spectra in starlike domains using the Vekua integral operator and singular value minimization

Alexandre Demidov[1] and Dmitry Lyakhov[2*†]

[1]Lomonosov Moscow State University, Leninskie Gory, 1, Moscow, 119991, Russia.
[2]RUDN University, Miklukho-Maklaya, 6, Moscow, 117198, Russia.

*Corresponding author(s). E-mail(s): dmlyakhov@gmail.com;
Contributing authors: demidov.alexandre@gmail.com;
†These authors contributed equally to this work.

**Abstract**

This paper introduces a highly efficient, fully vectorized, mesh-free computational framework for solving the Laplace eigenvalue problem within $\boldsymbol{d}$-dimensional star-shaped domains under homogeneous Dirichlet and approximate Robin boundary conditions. Moving away from unstable classical point-matching collocation and costly domain-based discretizations, the proposed method leverages a regularized formulation of Vekua's integral operators to map harmonic polynomials directly onto the Helmholtz solution space without boundary kernel singularities. We construct a fast, tensor-based assembly scheme utilizing Gauss–Legendre and spherical quadratures, completely eliminating nested internal loops in Python/NumPy implementations. The detection of true spectral parameter values $\boldsymbol{\lambda = k^2}$ and the robust diagnosis of mode multiplicities (degenerate modes) are achieved via singular value decomposition (SVD) minimization and clustering of the lowest singular values. Spurious modes are systematically filtered out using explicit a posteriori error bounds computed via the Barnett–Fox–Henrici–Moler (FHM) framework. Numerical experiments on non-canonical 2D geometries (circles, squares, ellipses under continuous deformation, and highly non-convex multi-lobe stars) demonstrate that the SVD-driven boundary solver achieves identical spectral precision to conventional finite element methods (FEM) while

reducing the discrete problem's dimensionality by over three orders of magnitude (operating on a compact $\mathbf{31 \times 31}$ matrix vs. 50,000+ degrees of freedom in commercial packages). Finally, the utility of the precomputed natural eigenbasis as a rapid computational engine for global spectral Galerkin methods in elliptic partial differential equations is discussed.

**Keywords:** Laplace eigenproblem, Vekua integral operators, Singular value decomposition, Tensor-based vectorization, Mesh-free boundary methods, Barnett-FHM error bounds

**MSC Classification:** 65N25 , 65R20 , 15A18 , 35P05

# 1 Introduction

The problem of determining the eigenvalues and eigenfunctions of the Laplace operator subject to homogeneous Robin (and, in particular, Dirichlet) boundary conditions is a classical problem in mathematical physics. It routinely arises in modeling membrane vibrations, acoustic modes, quantum wells, and diffusion processes. While solutions in canonical domains admit explicit analytical formulations, arbitrary geometries necessitate the use of numerical methods. One such approach is the Ritz method (1908), where an approximate solution is constructed using basis functions that satisfy the boundary conditions but not necessarily the governing differential equation. In 1926, Erich Trefftz (1888–1937) proposed a dual concept: utilizing basis functions that strictly satisfy the differential equation instead. Regarding the boundary conditions, Fox, Henrici, and Moler (FHM) [1] proposed satisfying them only at appropriately pre-allocated boundary nodes, a strategy that gave rise to the term "collocation method" (from the Latin *collocatio*, meaning placement).

However, the classical point-matching collocation method suffers from the emergence of spurious eigenvalues and a catastrophic loss of matrix conditioning as the number of basis functions increases. Another profound difficulty is associated with the inherent instability of conventional techniques that evaluate the eigenvalues $\lambda$ of the discrete boundary residual matrix $A$ by searching for the roots of the characteristic

determinant $\det(A - \lambda I)$. Meanwhile, for star-shaped domains, the idea [2] emerged to utilize Vekua's integral formulas [3] and their generalization to the multidimensional case [4], offering a robust alternative to conventional method of fundamental solutions [5–7] and modern high-precision polygonal solvers [8].

Vekua's formulas map harmonic functions onto solutions of the Helmholtz equation $\Delta v + k^2 v = 0$, where $\lambda = k^2$ represents the eigenvalue and $k > 0$ is the wavenumber. Such basis functions vary from harmonic polynomials for simple domains to fundamental solutions with fictitious sources and allow the solution to satisfy the Dirichlet or Robin boundary conditions. However, the practical application of Vekua's formulas requires overcoming significant computational hurdles due to the singularity in the integral kernel, which leads to severe matrix ill-conditioning. The present work proposes a unified computational framework that successfully addresses these long-standing issues.

Our primary contributions can be summarized as follows:

- *Regularization and assembly.* We derive a regularized form of the Vekua integral operator that completely eliminates the kernel singularity. Based on this formulation, an efficient tensor-based computational scheme is constructed to evaluate the boundary residual matrix using Gauss–Legendre quadratures.
- *Basis generation.* The basis in the solution space of the Helmholtz equation is not selected arbitrarily or blindly (such as plane waves or Bessel functions). Instead, it is explicitly constructed from harmonic polynomials via Vekua's formulas, naturally aligning with the polar parametrization of the star-shaped boundary. For the geometries under consideration, the degree of these polynomials remains small, ensuring high accuracy of the numerical results.
- *SVD filtration.* The target eigenvalues are determined not by searching for the unstable roots of the characteristic determinant, but by minimizing and subsequently clustering the lowest singular values of the residual matrix. This framework allows

for the simultaneous detection of eigenvalue multiplicities (degenerate modes) while reliably monitoring the computational stability and conditioning of the system.

The proposed approach is not intended as a universal replacement for the conventional finite element method (FEM) in arbitrary geometries. Rather, it represents a highly efficient, specialized boundary-focused tool for star-shaped domains. The method completely shifts the computational complexity of the problem from the domain's volume to its boundary, significantly reducing the dimensionality of the discrete problem.

Furthermore, the developed efficient eigenfunction solver for arbitrary star-shaped domains opens new avenues for a broader revitalization of global spectral Galerkin methods. Traditionally, global spectral methods have been constrained to canonical geometries due to their reliance on standard orthogonal bases, such as Chebyshev or Legendre polynomials [9]. The framework presented here enables the precomputation of precise, "natural" eigenfunctions inherent to the specific domain. These custom eigenfunctions can then serve as an optimal, tailored basis for solving a wide class of subsequent boundary value problems via the Galerkin method, thereby preserving spectral convergence rates on non-classical geometries.

## 2 Vekua Formula and Basis Functions

Let $u$ be a harmonic function in a domain $\Omega \Subset \mathbb{R}^d$ that is starlike with respect to the origin, let $r = |x|$ be the distance from $x = 0$ to $x \in \Omega$, let $k > 0$ be the so-called wavenumber, and let $J_1$ be the Bessel function of the first kind of order one. The Vekua formula [3], [4]

$$V[u(x)] = u(x) - \int_0^1 \frac{k|x|}{2} \frac{t^{d/2-1}}{\sqrt{1-t}} J_1(k|x|\sqrt{1-t}) u(xt)\, dt \tag{1}$$

transforms the harmonic function $u$ into a solution $V[u] : \Omega \ni x \mapsto V[u(x)]$ of the Helmholtz equation $\Delta V[u] + k^2 V[u] = 0$. As noted above, a certain difficulty in applying the Vekua formula is related to the singularity in the integral kernel as $t \to 1$. This difficulty is easily eliminated. The substitution $s = \sqrt{1-t}$ leads to the following regular Vekua formula:

$$V[u(x)] = u(x) - \int_0^1 \underbrace{k|x|(1-s^2)^{d/2-1} J_1(k|x|s)}_{\text{Regular kernel}} u\big((1-s^2)x\big) ds\,, \tag{2}$$

This formula contains no singularities and is perfectly suited for numerical integration.

Note that the Vekua operator $V : u \mapsto V[u]$ (2) is invertible and maps classical harmonic polynomials $u_n$ (which form the so-called Laplace basis for harmonic functions) into generalized harmonic Helmholtz polynomials $v_n = V[u_n]$ with a given wavenumber $k$ (forming the corresponding basis in the solution space of the Helmholtz equation). Thus, the desired eigenfunction $V(x)$ can be represented as a linear combination

$$V(x) = \sum c_n v_n(x) \tag{3}$$

in terms of the basis functions $v_n = V[u_n]$. By varying the coefficients $c_n$ (control parameters), one can approximate with any desired accuracy the eigenfunction of the Laplace operator subject to the Dirichlet boundary condition, as well as approximate (for example, by the collocation method or the method of least squares) the Robin condition.

# 3 Boundary Residual Discretization and Tensor-Based Computational Scheme

To implement the method numerically, the continuous boundary condition must be discretized. In the two-dimensional case (d = 2), we define $M$ collocation points $x_i =$

$(\rho(\theta_i)\cos\theta_i, \rho(\theta_i)\sin\theta_i)$ along the contour $\Gamma$, where $\theta_i$ represents the polar angle grid $(i = 1, \ldots, M)$, and let $N_h$ denote the total number of harmonics used. The problem then reduces to analyzing a rectangular boundary residual matrix $A(k) \in \mathbb{R}^{M\times N_h}$.

To evaluate the integral in the regularized Vekua form (2), the Gauss–Legendre quadrature rule featuring $Q$ nodes $s_q$ and weights $w_q$ on the interval $[0, 1]$ is employed. For each boundary point $x_i$ and each transformed harmonic $u_n$, the fundamental element of the matrix $A(k)$ is constructed as follows:

$$A_{i,n}(k) = u_n(x_i) - \sum_{q=1}^{Q} w_q \cdot \left[k|x_i|J_1(k|x_i|s_q) \cdot u_n\big(x_i(1 - s_q^2)\big)\right]. \tag{4}$$

However, the direct application of formula (4) with a uniform grid over $\theta$ is efficient only for canonical domains such as a circle or an ellipse. When transitioning to complex star-shaped geometries featuring narrow lobes or sharp corners (e.g., multi-ray stars or a square), a uniform angular step causes the collocation points to be distributed too sparsely on the protrusions and excessively densely in the recesses. In such scenarios, the SVD algorithm will artificially overemphasize the residual in the recesses while neglecting the error on the protrusions. Consequently, this leads to a degradation of the boundary condition fulfillment at the periphery, causing the algorithm to either skip true eigenvalues or generate spurious modes.

To mitigate this effect, a geometric row-weighting procedure is introduced. The classical boundary arc element is defined as $ds = \sqrt{\rho(\theta)^2 + \rho'(\theta)^2}d\theta$. In the software implementation, to avoid symbolic or numerical differentiation of $\rho(\theta)$, we transition to Cartesian coordinates and approximate the arc element via the chord lengths between adjacent points:

$$\Delta s_{i,i-1} = \sqrt{(x_i - x_{i-1})^2 + (y_i - y_{i-1})^2}. \tag{5}$$

Then, the integral weight $W_i$ for the $i$-th collocation point is computed as the average of the adjacent chord lengths:

$$W_i = \frac{\Delta s_{i,i-1} + \Delta s_{i,i+1}}{2}. \tag{6}$$

This approach guarantees an accurate and adaptive description of sharp corners and localized boundary deformations. The final regularization of the matrix $A(k)$ is achieved by multiplying each of its $i$-th rows by the weighting factor $\sqrt{W_i}$.

To ensure high computational performance and completely eliminate nested loops, the assembly of the matrix $A(k)$ is executed using vectorized tensor operations. For this purpose, three-dimensional tensors of size $(M \times N_h \times Q)$ are constructed, representing the values of the basis functions at all quadrature nodes simultaneously. In terms of tensor algebra, the assembly scheme is formulated as:

$$A(k) = U_{\text{boundary}} - (\text{Kernel} \odot U_{\text{tensor}}) \times_3 \mathbf{w}, \tag{7}$$

where $U_{\text{boundary}} \in \mathbb{R}^{M \times N_h}$ is the matrix containing the values of the primal harmonics on the boundary; $\text{Kernel} \in \mathbb{R}^{M \times N_h \times Q}$ is the tensor of the evaluated regular Vekua kernel values; $U_{\text{tensor}} \in \mathbb{R}^{M \times N_h \times Q}$ is the tensor of the harmonic values at the internal scaling points $(1 - s_q^2)x_i$; the symbol $\odot$ denotes the element-wise (Hadamard) product along the respective axes, and $\times_3 \mathbf{w}$ specifies the tensor contraction (weighted summation) along the third mode with the Gauss–Legendre weight vector $\mathbf{w} = [w_1, \ldots, w_Q]^T$.

In the three-dimensional case ($d = 3$), the boundary of a starlike domain is topologically equivalent to a sphere and can be uniquely projected onto it via rays from

the center of starlikeness. Finally, to efficiently compute the regularized Vekua integral in 3D space instead of polar quadratures, high-precision V.I. Lebedev spherical quadrature formulas [10, 11] are applied.

### 3.1 Singular Value Decomposition and Multiplicity Diagnosis

For a specified wavenumber $k$, the boundary residual matrix $A(k) \in \mathbb{R}^{M\times N_h}$ maps the unknown coefficient vector $\mathbf{c}$ to the discrete residual along the contour $\Gamma$. To identify non-trivial solutions, we formulate the problem as minimizing the norm of the boundary residual on the unit sphere:

$$\min_{\|\mathbf{c}\|_2=1} \|A(k)\mathbf{c}\|_2 \,. \tag{8}$$

According to matrix computation theory [12, 13], the solution to (8) is inherently governed by the singular value decomposition (SVD) of the matrix: $A(k) = U\Sigma V^T$. The rectangular matrix $\Sigma$ contains non-negative singular values ordered monotonically: $\sigma_1 \geq \sigma_2 \geq \cdots \geq \sigma_{N_h}$. The minimum singular value, defined as $\sigma_{\min}(k) = \sigma_{N_h}$, quantifies the proximity of $A(k)$ to a rank-deficient state.

The geometric interpretation of this SVD minimization framework is highly intuitive. For a fixed wavenumber $k$, the matrix $A(k)$ maps the unit sphere from the normalized coefficient space ($\|\mathbf{c}\|_2 = 1$) into a hyperellipsoid within the boundary residual space $\mathbb{R}^M$. The singular values represent the lengths of the semi-axes of this hyperellipsoid. Geometrically, the smallest singular value $\sigma_{N_h}$ corresponds to the shortest distance from the origin to the surface of the hyperellipsoid. Consequently, tracking an eigenvalue $\lambda = k^2$ reduces to scanning the parameter $k$ to locate points where the hyperellipsoid "flattens" and intersects the origin, i.e., $\sigma_{N_h}(k) \to 0$ within numerical tolerance.

When the two smallest semi-axes vanish simultaneously ($\sigma_{N_h} \approx 0$ and $\sigma_{N_h-1} \approx 0$), the hyperellipsoid degenerates into a disk, which geometrically signifies a two-fold degeneracy (multiplicity) of the eigenmode. To ensure robust automated detection of such multiple roots, the algorithm validates the following conditions:

$$\frac{\sigma_{N_h}}{\sigma_{N_h-1}} \approx 1 \quad \text{and} \quad \frac{\sigma_{N_h-2}}{\sigma_{N_h-1}} \gg 1\,. \tag{9}$$

The coefficient vectors $\mathbf{c}$ corresponding to these orthogonal modes are directly extracted from the final columns of the right singular vector matrix $V$. Thus, the SVD framework serves not only as a high-performance computational engine but also as an elegant geometric indicator of the spectral structure on the domain's boundary.

Once the true wavenumber $k$ and its associated coefficient vector $\mathbf{c} = [c_1, \ldots, c_{N_h}]^T$ are determined, the reconstruction of the continuous eigenfunction $u(x)$ inside the domain $\Omega$ is performed on a regular field grid $x_f = (r_f, \theta_f)$. This volume reconstruction is identical to the boundary evaluation process:

$$u(x_f) = \sum_{j=1}^{N_h} c_j \cdot \left[ v_j(x_f) - \int_0^1 k|x_f| J_1(k|x_f|s) v_j\big((1-s^2)x_f\big)\, ds \right], \tag{10}$$

where $v_j(x)$ represents the primal harmonic polynomial (the Laplace basis). The expression enclosed in brackets is evaluated utilizing the exact same tensor-based Gauss–Legendre scheme (7), eliminating nested internal loops and ensuring rapid field restoration across the entire domain.

## 3.2 Properties of the Minimum Singular Value and Choice of Computational Parameters

Since the boundary residual matrix $A(k)$ is constructed from the values of normalized basis functions and their integral transformations along the contour $\Gamma$, the minimum

singular value $\sigma_{\min}(A(k))$ is strictly dimensionless. Consequently, $\sigma_{\min}$ serves as a universal, relative diagnostic indicator of the boundary boundary mismatch rather than a physical quantity possessing dimension.

The free parameters of the proposed method include: $Q$ — the order of the Gauss–Legendre quadrature, $M$ — the number of boundary collocation points, $N_h$ — the number of primal harmonics (the dimensionality of the target coefficient vector $\mathbf{c}$), and $N_k$ — the number of discrete sampling points for the wavenumber $k$. Numerical experiments indicate that for domains with smooth boundaries, the initial parameters should satisfy the condition $M \geq 6N_h$, resulting in a highly overdetermined linear system. For geometries characterized by sharp corners, high aspect ratios, or rapidly varying shapes, a greater degree of overdetermination is required, typically $M \approx 10N_h$–$14N_h$. Furthermore, in the presence of boundary singularities (such as vertices), it is highly beneficial to couple the row-weighting procedure (6) with a localized clustering of collocation points along the arc length in the vicinity of the corners.

The selection of the quadrature order $Q$ depends heavily on the target wavenumber range $k$. For moderate values ($k \leq 10$) and quasi-circular domains ($\max \rho \leq 2$), the Gauss–Legendre quadrature rule with $Q \geq 60$ ensures machine precision. However, as $k$ or the maximum radial extent of the domain increases, the quadrature order must be scaled accordingly because the underlying Vekua kernel, which contains the Bessel function $J_1(krs)$, exhibits high-frequency oscillations over the integration interval $s \in [0, 1]$.

The scanning interval for the spectral parameter $k$ can be efficiently constrained by invoking the monotonicity property of eigenvalues with respect to the domain inclusion. If a star-shaped domain $\Omega$ is strictly bounded between two concentric circles of inscribed radius $R_{\text{in}}$ and circumscribed radius $R_{\text{out}}$ ($R_{\text{in}} \leq \rho(\theta) \leq R_{\text{out}}$), the first

fundamental mode $k_1$ is guaranteed to lie within the interval:

$$k_1 \in \left[ \frac{j_{0,1}}{R_{\text{out}}}, \frac{j_{0,1}}{R_{\text{in}}} \right], \tag{11}$$

where $j_{0,1} \approx 2.4048$ denotes the first positive zero of the Bessel function $J_0(z)$. For higher-order modes, this search interval is expanded to the right and sequentially scanned using a coarse grid for $k$. This grid is subsequently refined locally (down to a step size of $\Delta k \sim 10^{-8}$) in the immediate neighborhoods of the detected local minima of the function $\sigma_{\min}(A(k))$.

### 3.3 A Posteriori Accuracy Estimation and Spurious Mode Filtering

An a posteriori evaluation of the computational accuracy is performed utilizing Barnett's method [14], which is fundamentally rooted in the classical Fox–Henrici–Moler (FHM) theorem [1] and the rigorous operator bounds established by Moler and Payne [15]. Once a target eigenvalue $\lambda = k^2$ and its corresponding eigenfunction $u(r, \theta)$ have been determined, we compute the boundary $L_2$-norm along the contour $\partial\Omega$ (incorporating the previously defined geometric weights $W_i$):

$$\|u\|_{L_2(\partial\Omega)} = \left( \oint_{\partial\Omega} |u(s)|^2 \, ds \right)^{1/2}, \tag{12}$$

alongside the domain $L_2$-norm $\|u\|_{L_2(\Omega)}$ evaluated in polar coordinates:

$$\|u\|_{L_2(\Omega)} = \left( \int_0^{2\pi} \int_0^{\rho(\theta)} |u(r, \theta)|^2 r \, dr \, d\theta \right)^{1/2}. \tag{13}$$

For the star-shaped domains under consideration, which are naturally parametrized by the radial function $\rho(\theta)$, the domain integral formulation is ideally suited for high-order tensor-product Gauss–Legendre quadrature rules.

Consequently, the sharp a posteriori error bound $\eta$ is formulated as follows:

$$\eta = \sqrt{\lambda}\frac{\|u\|_{L_2(\partial\Omega)}}{\|u\|_{L_2(\Omega)}}\,. \tag{14}$$

According to the FHM theorem, the exact analytical eigenvalue $\lambda_{\text{true}}$ is guaranteed to reside within the rigorous interval:

$$\lambda_{\text{true}} \in [\lambda - \eta,\, \lambda + \eta]\,. \tag{15}$$

Furthermore, the error bound (14) serves as a robust filter against spurious (false) eigenvalues. If a detected root $k$ is spurious, the reconstructed function $u(r,\theta)$ vanishes or degenerates not only along the boundary $\partial\Omega$ but also across the entire internal domain. As a direct consequence, the domain norm $\|u\|_{L_2(\Omega)}$ becomes extremely small, causing the ratio $\eta$ to spike drastically to large values (typically $10^4$ or higher). Conversely, for a true physical eigenvalue, the ratio $\eta$ remains strictly small (approaching machine precision).

Additionally, to verify the structural integrity of the computed eigenfunctions in the subsequent sections, we monitor the normalized $L_2$-residual of the governing differential equation within the domain interior:

$$\epsilon_{\text{res}} = \frac{\|\Delta u + k^2 u\|_{L_2(\Omega)}}{\|u\|_{L_2(\Omega)}}\,, \tag{16}$$

which provides an independent check on the validity of the analytic continuation.

# 4 Numerical Results and Algorithm Verification

The numerical pipeline of the proposed tensor-based framework was implemented in Python utilizing the standard high-performance `NumPy` and `SciPy` libraries. The validation hierarchy of the computational experiments is structured systematically as follows. First, we present the spectral computation results for canonical geometries that admit exact analytical solutions: a unit circle and a square. This initial step serves to rigorously evaluate the ultimate precision and convergence rates of the method.

Second, we explore the spectral characteristics of elliptical domains with a dynamically varying aspect ratio, demonstrating the algorithm's capability to automatically detect and track the splitting of degenerate modes. The final and most challenging benchmark assesses the eigenvalue computation and volume eigenfunction reconstruction for a two-lobe and seven-lobe star-shaped domains.

Unless specified otherwise, all numerical simulations are carried out utilizing a uniform baseline configuration of computational parameters: the Gauss–Legendre quadrature order $Q = 60$, the number of primal Laplace harmonics $N_h = 15$, the number of boundary collocation points $M = 200$, and the number of wavenumber sampling points $N_k = 800$ within the a priori scanning interval $k \in [1.5, 10.0]$.

For each representative test case, the comprehensive summary tables provide the following details: the mode index, the eigenvalue multiplicity, the exact theoretical benchmark (where available), the computed numerical eigenvalue, and the corresponding sharp a posteriori error bound $\eta$ derived via the Barnett–FHM framework (14). For the two-lobe and seven-lobe star-shaped domains, the normalized $L_2$-residual within the interior is also presented.

## 4.1 Unit Circle

For the unit circle, the exact analytical eigenvalues $k_{m,p}$ correspond to the roots of the Bessel functions of the first kind satisfying the condition $J_m(k) = 0$. The computed numerical results along with the theoretical benchmarks are presented in Table 1.

**Table 1** Eigenvalues for the unit circle.

| No. | $\lambda_{\text{exact}}$ | $\lambda_{\text{SVD}}$ | Mult. | Apost. Error $\eta$ |
|---|---|---|---|---|
| 1 | 5.7832 | 5.7832 | 1 | $6.43 \times 10^{-6}$ |
| 2 | 14.6820 | 14.6820 | 2 | $1.13 \times 10^{-5}$ |
| 3 | 26.3746 | 26.3746 | 2 | $1.46 \times 10^{-5}$ |
| 4 | 30.4713 | 30.4712 | 1 | $1.56 \times 10^{-5}$ |
| 5 | 40.7065 | 40.7065 | 2 | $2.92 \times 10^{-6}$ |
| 6 | 49.2185 | 49.2184 | 2 | $2.46 \times 10^{-5}$ |
| 7 | 57.5829 | 57.5829 | 2 | $2.04 \times 10^{-5}$ |

Figure 1 illustrates representative examples of eigenfunctions corresponding to a two-fold eigenvalue degeneracy. It is clearly observed that the computed functions are linearly independent and mutually orthogonal, which strictly complies with the theoretical foundations.

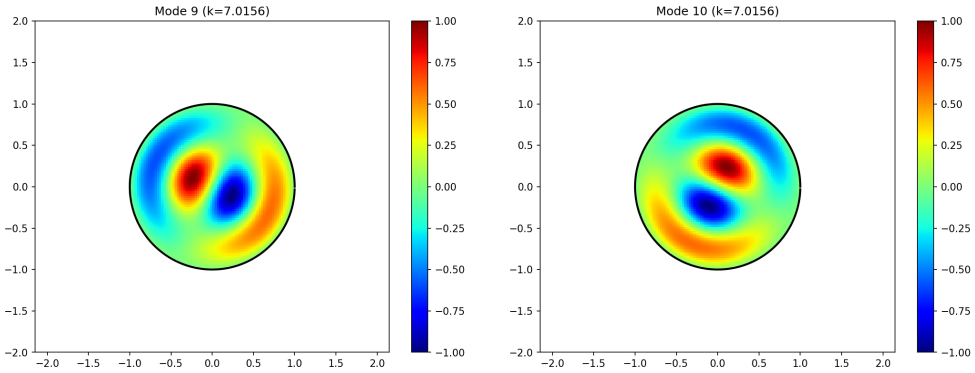



**Fig. 1** Two-fold degenerate eigenfunctions corresponding to the eigenvalue $\lambda = 49.2185$ for the unit circle.

## 4.2 Square Domain

Numerical simulations are carried out for a square domain with side length $a = 2$. The exact analytical eigenvalues are evaluated according to the classical formula:

$$k_{m,n} = \frac{\pi}{2}\sqrt{m^2 + n^2}\,, \tag{17}$$

where $m, n \in \mathbb{N}$ represent the wave mode indices. The computed numerical results along with the theoretical benchmarks are summarized in Table 2.

**Table 2** Eigenvalues for the square domain.

| No. | $\lambda_{\text{exact}}$ | $\lambda_{\text{SVD}}$ | Mult. | Apost. Error $\eta$ |
|---|---|---|---|---|
| 1 | 4.9348 | 4.9348 | 1 | $1.636 \times 10^{-7}$ |
| 2 | 12.3370 | 12.3370 | 2 | $2.287 \times 10^{-6}$ |
| 3 | 19.7392 | 19.7392 | 1 | $2.429 \times 10^{-6}$ |
| 4 | 24.6740 | 24.6740 | 2 | $2.628 \times 10^{-6}$ |
| 5 | 32.0762 | 32.0763 | 2 | $4.041 \times 10^{-5}$ |
| 6 | 41.9458 | 41.9458 | 2 | $1.400 \times 10^{-4}$ |
| 7 | 44.4132 | 44.4132 | 1 | $1.921 \times 10^{-3}$ |

## 4.3 Elliptical Domain

Initial numerical simulations are carried out for an elliptical domain with semi-axes $a = 2.0$ and $b = 1.0$. The computed spectral data are presented in Table 3. For all identified modes, the multiplicity is strictly equal to 1. Due to the absence of exact analytical closed-form solutions for this geometry, the table provides exclusively the computed numerical eigenvalues alongside their corresponding a posteriori error bounds $\eta$.

To validate the structural accuracy and sensitivity of the developed numerical algorithm, we solved a benchmark problem investigating the splitting of two-fold

**Table 3** Eigenvalues for the elliptical domain.

| No. | $\lambda_{\mathrm{SVD}}$ | Mult. | Apost. Error $\eta$ |
|---|---|---|---|
| 1 | 6.2754 | 1 | $1.094 \times 10^{-6}$ |
| 2 | 10.0284 | 1 | $3.369 \times 10^{-6}$ |
| 3 | 11.7367 | 1 | $6.234 \times 10^{-7}$ |
| 4 | 14.8773 | 1 | $9.956 \times 10^{-7}$ |
| 5 | 15.9240 | 1 | $4.242 \times 10^{-6}$ |
| 6 | 21.0230 | 1 | $1.090 \times 10^{-5}$ |
| 7 | 24.8857 | 1 | $1.243 \times 10^{-5}$ |

degenerate eigenvalues of the Laplace operator under homogeneous Dirichlet boundary conditions as a circular domain is deformed into an ellipse. In order to enforce a strict area-preserving constraint ($S = \pi$) across all continuous deformations, the semi-axes of the ellipse were parameterized as follows:

$$a = \frac{1}{\sqrt{1+\epsilon}} \quad b = \sqrt{1+\epsilon}$$

.

The ellipse with semi-axes $a$ and $b$ is explicitly defined in polar coordinates as follows:

$$\rho(\theta) = \frac{a \cdot b}{\sqrt{(b \cdot \cos\theta)^2 + (a \cdot \sin\theta)^2}} \,. \tag{18}$$

According to Hadamard's variational formula within shape perturbation theory [16], breaching the rotational symmetry of a domain induces a splitting of degenerate eigenvalues that is linear with respect to the perturbation parameter $\epsilon$—a classical phenomenon that serves as a cornerstone for studying the normal oscillations of elliptical planets [17], the eigenfrequencies of non-canonical membranes [18], and high-precision asymptotic boundary variations [19]. For the chosen parameterization, the first-order boundary displacement is given by $\delta R(\theta) \approx -\frac{1}{2}\epsilon\cos(2\theta)$. This formulation yields a theoretical slope for the splitting magnitude, $\Delta\lambda/\epsilon$, which strictly approaches

the unperturbed eigenvalue in the limit as $\epsilon \to 0$:

$$\lim_{\epsilon \to 0} \frac{\Delta\lambda}{\epsilon} = \lambda_0 \,. \tag{19}$$

The numerical results modeling the evolution of these eigenvalues computed via the proposed Vekua framework are summarized in Table 4.

**Table 4** Laplace operator eigenvalues for the elliptical domain under varying deformation parameter $\epsilon$.

| Eigenmode | $\epsilon = -0.01$ | $\epsilon = 0.01$ |
|---|---|---|
| 1 | 5.7835 | 5.7835 |
| 2 | 14.6089 | 14.6096 |
| 3 | 14.7564 | 14.7557 |
| 4 | 26.3663 | 26.3665 |
| 5 | 30.4822 | 30.4820 |
| 6 | 40.7027 | 40.7027 |
| 7 | 48.9789 | 48.9812 |
| 8 | 49.4733 | 49.4707 |
| 9 | 57.5787 | 57.5788 |
| 10 | 70.7955 | 70.7965 |

For the fundamental two-fold degenerate mode ($m = 1, n = 1$), the unperturbed numerical eigenvalue was found to be $\lambda_0 = 14.6820$, which closely matches the theoretical benchmark $j_{1,1}^2 \approx 14.6819$. Under a boundary deformation of $\epsilon = 0.0100$, the computed numerical splitting magnitude was $\Delta\lambda = 0.1461$, yielding an empirical slope of $\Delta\lambda/\epsilon = 14.6100$. The excellent agreement between these numerical results and the first-order predictions of shape perturbation theory strictly validates the correctness and robust convergence of the developed framework when resolving continuous boundary perturbations.

Additionally, the convergence properties of the method were scrutinized on higher-order multiple eigenvalues. For the degenerate mode $m = 1, n = 2$ ($\lambda_0 = 49.2182$) under the same deformation of $\epsilon = 0.0100$, the numerical splitting was evaluated as

$\Delta\lambda = 0.4895$. This corresponds to a slope of $\Delta\lambda/\epsilon = 48.9500$, deviating from the theoretical unperturbed value $\lambda_0$ by less than 0.5%.

Concurrently, for the multiple eigenvalue $m = 2, n = 1$ ($\lambda_0 = 26.3746$), first-order perturbation theory predicts that the splitting magnitude must be identically zero. This stems from the fact that the angular harmonic of the elliptical deformation ($k = 2$) fails to satisfy the resonant splitting condition, $2m = k$, for this particular mode. The numerical simulations strongly corroborate this theoretical prediction: at $\epsilon = 0.0100$, the computed splitting was a mere $\Delta\lambda = 0.0002$, which clearly indicates a higher-order behavior of $\mathcal{O}(\epsilon^2)$. These numerical experiments explicitly demonstrate the high physical fidelity of the developed framework and its unique capacity to accurately replicate the fine spectral structure of the Laplace operator upon symmetry breaking.

### 4.4 Arbitrary Star-Shaped Domain

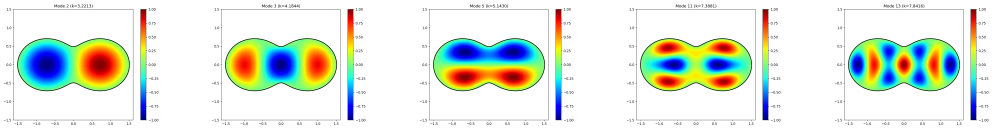
Suppose that the boundary of the domain $D$ is parameterized in polar coordinates by the following radial function:

$$\rho(\theta) = 1.0 + \delta \cdot \cos(N_L \cdot \theta) \tag{20}$$

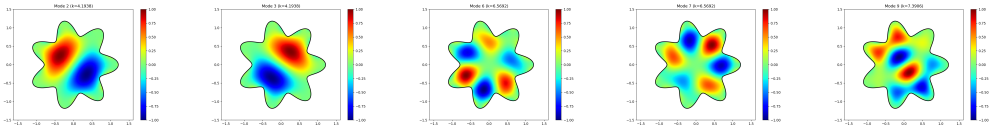
where $\delta$ is the perturbation amplitude, and $N_L$ denotes the number of lobes.

Figure 2 illustrates the reconstructed eigenfunctions along with their corresponding eigenvalues for star-shaped domains parameterized by $N_L = 2, \delta = 0.51$ and $N_L = 7, \delta = 0.21$, respectively. For each computed eigenvalue and its associated eigenfunction, both the sharp Barnett a posteriori error bound $\eta$ and the normalized $L_2$-residual $\epsilon_{\text{res}}$ within the domain interior are provided.

Table 5 outlines the computed spectral data for the star-shaped domain configuration with perturbation amplitude $\delta = 0.21$ and $N_h = 7$ lobes.



$\lambda = 10.376$ $\eta = 0.051$ $\epsilon_{res} = 0.0006$ | $\lambda = 17.509$ $\eta = 0.137$ $\epsilon_{res} = 0.001$ | $\lambda = 26.451$ $\eta = 0.075$ $\epsilon_{res} = 0.002$ | $\lambda = 54.584$ $\eta = 0.054$ $\epsilon_{res} = 0.007$ | $\lambda = 61.491$ $\eta = 0.117$ $\epsilon_{res} = 0.008$



$\lambda = 17.588$ $\eta = 0.343$ $\epsilon_{res} = 0.003$ | $\lambda = 17.588$ $\eta = 0.343$ $\epsilon_{res} = 0.005$ | $\lambda = 43.154$ $\eta = 0.612$ $\epsilon_{res} = 0.003$ | $\lambda = 43.154$ $\eta = 0.612$ $\epsilon_{res} = 0.003$ | $\lambda = 54.621$ $\eta = 0.368$ $\epsilon_{res} = 0.006$

**Fig. 2** Selected eigenmodes for the star-shaped domains. Each subplot displays the corresponding numerical eigenvalue, the sharp Barnett a posteriori error bound $\eta$, and the normalized internal $L_2$-residual $\epsilon_{\text{res}}$, with the degenerate eigenmodes for the 7-lobe geometry distinctly visualized.

**Table 5** Laplace operator eigenvalues for the star-shaped domain under parameters $\delta = 0.21$ and $N_h = 7$.

| Mode index | $\lambda$ | Multiplicity | A posteriori error $\eta$ | $\epsilon_{\text{res}}$ |
|---|---|---|---|---|
| 1 | 6.9447 | 1 | 0.227 | 0.003 |
| 2 | 17.5881 | 2 | 0.344 | 0.005 |
| 3 | 30.5162 | 2 | 0.553 | 0.002 |
| 4 | 43.1548 | 2 | 0.612 | 0.003 |
| 5 | 54.6212 | 2 | 0.367 | 0.006 |
| 6 | 66.1837 | 2 | 0.551 | 0.006 |
| 7 | 69.2343 | 2 | 0.851 | 0.006 |

The identified multiple (degenerate) eigenvalues were successfully replicated and validated through independent finite element method (FEM) simulations.

## 5 Comparison with the Finite Element Method

To evaluate the performance of the proposed framework against standard state-of-the-art numerical suites, we present a comparative spectral analysis for the unit circle, the square domain, and the seven-lobe star-shaped geometry using the COMSOL

Multiphysics© software package (version 6.4). The finite element method (FEM) simulations were executed utilizing conventional linear Lagrange elements coupled with the built-in ARPACK eigenvalue solver. The corresponding summary tables outline the computed eigenvalues alongside the total number of degrees of freedom (DOFs) across three distinct mesh refinement levels: *Coarse*, *Normal*, and *Extremely Fine*.

Crucially, under the baseline configuration of computational parameters specified above, the dimensions of the boundary residual matrix for our SVD-based algorithm remain strictly fixed at $31 \times 31$, corresponding to a mere $DOFs = 31$ for the discretized problem. The benchmark results obtained via the COMSOL package are summarized in Table 6.

**Table 6** Computation of the first three eigenvalues via the conventional finite element method (FEM) in COMSOL.

| Geometry | Grid | DOF | $\lambda$ |
|---|---|---|---|
| Circle | Coarse | 533 | 5.8227 |
| | | | 14.785 |
| | | | 26.570 |
| | Normal | 1137 | 5.8004 |
| | | | 14.726 |
| | | | 26.456 |
| | Extremely Fine | 51393 | 5.7836 |
| | | | 14.683 |
| | | | 26.376 |
| Square | Coarse | 577 | 4.9349 |
| | | | 12.339 |
| | | | 19.747 |
| | Normal | 1217 | 4.9348 |
| | | | 12.337 |
| | | | 19.741 |
| | Extremely Fine | 50225 | 4.9348 |
| | | | 12.337 |
| | | | 19.739 |
| star-shape domain $N_L = 7$ | Coarse | 2175 | 7.4116 |
| | | | 18.505 |
| | | | 32.161 |
| | Normal | 3593 | 7.4173 |
| | | | 18.516 |
| | | | 32.168 |
| | Extremely Fine | 50225 | 7.4218 |
| | | | 18.524 |
| | | | 32.171 |

Comparing the numerical benchmarks presented above with the results obtained via the proposed Vekua-SVD method in the preceding sections, it is evident that although the finite element method (FEM) within COMSOL formally provides higher precision at ultra-fine mesh levels ($DOFs > 50,000$), the proposed framework achieves comparable accuracy utilizing a mere $N_h = 31$ basis functions. Crucially, the discrepancies between the two approaches reside strictly within the limits of the computed sharp a posteriori error bounds $\eta$, confirming that the latter serves as a reliable mathematical indicator of solution accuracy.

The computational efficiency of the developed method is particularly pronounced when examining the reduction of degrees of freedom for geometrically complex domains. For the highly non-convex seven-lobe star-shaped geometry, the Vekua-SVD approach successfully captures the true eigenvalue spectrum and resolves the two-fold degenerate modes while operating on a highly compact $200 \times 31$ residual matrix (15 harmonic pairs plus the fundamental mode). In stark contrast, the commercial finite element suite required $DOFs = 50,225$ to achieve the equivalent spectral resolution. This reduction of the problem's dimensionality by more than three orders of magnitude (from $50,225$ to 31 unknowns) highlights the profound advantage of a paradigm shift from domain-based volume discretization to boundary-focused boundary formulations enabled by Vekua's analytic integral transformation.

Importantly, this transition does not compromise the reliability of the eigenvalue detection scheme, as the computed a posteriori error bounds provide a strict mathematical guarantee for the precision of the resulting solution. It must be emphasized that the Vekua-SVD framework inherently allows for the evaluation of such rigorous explicit error bounds. In contrast, this continuous boundary-driven error estimation approach is not directly applicable to conventional finite element schemes, since the

latter enforce boundary conditions pointwise or weakly across the mesh nodes, essentially satisfying them with machine precision at the boundary while masking the true analytical approximation error within the domain.

# 6 Vekua-SVD Framework as a Computational Engine for Elliptic Partial Differential Equations

Although the primary focus of this work is directed toward the precise evaluation of the Laplace operator spectrum, the numerical construction of the custom eigenfunction basis $\{u_j\}_{j=1}^{N_h}$ via the Vekua-SVD framework serves a much broader purpose. It fundamentally acts as a highly efficient, mesh-free computational engine for solving arbitrary linear elliptic boundary value problems (BVPs) within star-shaped domains.

Let us consider a general elliptic problem subject to an inhomogeneous Dirichlet boundary condition:

$$\mathcal{L}U = \Delta U + \alpha U = G(x,y), \quad U|_\Gamma = f(x,y)\,. \tag{21}$$

By decomposing the total solution into an extension function $U_0$ that satisfies the boundary data ($U_0|_\Gamma = f$) and a homogeneous correction $V$ ($V|_\Gamma = 0$), the latter can be rigorously expanded in terms of the precomputed eigenfunction basis: $V = \sum_j c_j u_j$. The modal coefficients $c_j$ are determined analytically via spectral projection:

$$c_j = \frac{\langle G - \mathcal{L}U_0,\, u_j \rangle_{L_2(\Omega)}}{\alpha - \lambda_j}\,, \tag{22}$$

where $\langle \cdot, \cdot \rangle_{L_2(\Omega)}$ denotes the standard inner product in $L_2(\Omega)$. Such a spectral reduction offers profound computational advantages.

For differential problems involving variable coefficients, e.g., $\Delta U + \sigma(x,y)U = G$, the globally analytic eigenfunction basis $\{u_j\}$ functions as an optimal trial space for

the global Galerkin method [9]. This reduces the governing partial differential equation (PDE) to a dense but remarkably low-dimensional algebraic system wherein the stiff Laplace operator is completely diagonalized. The elements of the resulting linear system ($\mathbf{Aw} = \mathbf{g}$) generated via the Galerkin projection are explicitly formulated as:

$$A_{k,j} = -\lambda_j \delta_{k,j} + \langle \sigma(x,y) u_k,\, u_j \rangle_{L_2(\Omega)}\,, \tag{23}$$

$$g_k = \langle G,\, u_k \rangle_{L_2(\Omega)}\,. \tag{24}$$

Because the basis functions $u_j$ analytically satisfy the Laplace operator mechanics, numerical integration is exclusively required to handle the variable coefficient $\sigma(x,y)$, which radically curtails the overall quadrature overhead. Inhomogeneous boundary conditions can, in turn, be seamlessly incorporated via the classical tau-method implementation [9].

Furthermore, this computational strategy extends naturally to time-dependent diffusion and wave propagation phenomena. The separation of space and time variables via the ansatz $U(x,y,t) = \sum T_j(t) u_j(x,y)$ yields independent ordinary differential equations (ODEs) governing the modal amplitudes. For instance, in chemical kinetics, assigning $G(x,y) = -k_r U$ models linear bulk reaction rates, whereas the Dirichlet constraint $U|_{\partial\Omega} = 0$ represents a perfectly absorbing catalytic boundary. In this context, the computed eigenvalues $\lambda_j$ directly dictate the characteristic diffusion relaxation time scales:

$$\tau_j = (D\lambda_j + k_r)^{-1}\,. \tag{25}$$

Analogously, the developed framework is inherently applicable to evaluating the critical cutoff frequencies of transverse magnetic (TM) modes in electromagnetic waveguides, as well as analyzing the complex geometrical structure of acoustics in irregular or fractal cavities [20, 21].

# 7 Conclusions

A reproducible, mesh-free computational framework has been developed for solving the Dirichlet Laplace eigenvalue problem within arbitrary star-shaped domains. The primary achievement of this study lies in the successful unification of a regularized Vekua integral transformation, a global harmonic Fourier–Bessel basis, a fully vectorized tensor-based quadrature assembly, and an SVD-driven minimization of the boundary mismatch. The critical methodological enhancements that ensured high computational stability include the implementation of discrete chord-based boundary arc-length weighting to maintain parameterization invariance, alongside strict explicit error monitoring via the Barnett–FHM-type formulation. This framework efficiently reduces the partial differential eigenvalue problem to a singular spectrum analysis of a compact boundary residual matrix $A(k)$. Consequently, the field quantities interior to the domain automatically satisfy the governing Helmholtz differential mechanics, while the fulfillment of the homogeneous Dirichlet boundary condition is controlled exclusively along the parameterized one-dimensional contour.

The proposed method is presented as a highly efficient, specialized computational tool tailored for radially bounded star-shaped geometries. Its competitive edge is convincingly demonstrated via a rigorous comparative benchmark against the conventional finite element method (FEM) implemented in COMSOL. The developed Vekua-SVD algorithm successfully extracts the target eigenvalues and perfectly captures two-fold degenerate modes (leveraging the natural symmetry of the underlying Fourier basis) utilizing a mere $N_h = 31$ basis functions, whereas the standard volume-based FEM requires over $50,000$ degrees of freedom (DOFs). This drastic dimensionality reduction by more than three orders of magnitude does not compromise the reliability of the spectral detection scheme, as the integrated a posteriori error bound functions as a robust mathematical filter against spurious roots. Furthermore, the precomputed spectral basis serves as a universal computational engine, enabling

one to directly solve arbitrary inhomogeneous elliptic boundary value problems without invoking domain-based grid discretizations.

Nevertheless, the fundamental limitations of the current method require critical reflection. The current mathematical formulation strictly mandates that the target domain must be star-shaped with respect to the chosen origin. Moreover, within standard double-precision arithmetic (`float64`), high-order Bessel functions exhibit numerical decay at lower frequencies, which inevitably constrains the resolution capacity of the basis when applied to boundaries characterized by high-frequency spatial variations. Crucially, the algorithm provides an honest and rigorous mathematical diagnosis of these boundaries: any onset of precision loss is immediately signaled by a sharp spike in the computed a posteriori error bound.

Future extensions of this methodology to highly non-convex shapes, generic Robin boundary operators, or differential models involving variable coefficients may leverage either a hybridization with conventional mesh-based schemes or a transition toward arbitrary-precision computational arithmetic.

## Declarations

- **Data availability:** Numerical data for the eigenspectra in this article are available from https://doi.org/10.5281/zenodo.24201676
- **Code availability:** Python code is available from the corresponding author on reasonable request
- **Ethics, Consent to Participate, and Consent to Publish declarations:** Not applicable.
- **Conflict of Interest / Competing Interests:** The authors declare that they have no competing financial or personal interests that could have appeared to influence the work reported in this paper.
- **Funding** Not applicable.

- **Author Contribution:**

  **Alexander Demidov**: Conceptualization, Methodology, Formal analysis, Theoretical analysis, Investigation, Writing – original draft, Supervision.

  **Dmitry Lyakhov**: Software, Validation, Numerical experiments, Data curation, Visualization, Software engineering, Writing – original draft, Writing – review & editing.

  All authors have read and agreed to the published version of the manuscript.

- **Acknowledgments** Not applicable.

## References

[1] Fox, L., Henrici, P., Moler, C.: Approximations and bounds for eigenvalues of elliptic operators. SIAM J. Numer. Anal. **4**, 89–102 (1967)

[2] Demidov, A.S.: Vekua's formula and the Construction of Eigenfuncitons and Eigenvalues of the Laplace Operator. In: Baturina, E.Y., Samsonyuk, O.N. (eds.) Proceedings of The 9th International School-Seminar Nonlinear Analysis and Extremal Problems, NLA-2026, pp. 31–32. ISDCT SB RAS, Irkutsk (2026)

[3] Vekua, I.N.: New Methods for Solving Elliptic Equations. North-Holland Series in Applied Mathematics and Mechanics, vol. 1. North-Holland Publishing Company & John Wiley & Sons, Amsterdam / New York (1967)

[4] Moiola, A., Hiptmair, R., Perugia, I.: Vekua theory for the Helmholtz operator. Z. Angew. Math. Phys. **62**, 779–807 (2011)

[5] Bogomolny, A.: Fundamental solutions method for elliptic boundary value problems. SIAM J. Numer. Anal. **22**, 644–669 (1985)

[6] Reutskiy, S.Y.: The method of fundamental solutions for eigenproblems with

Laplace and biharmonic operators. CMC **2**(3), 177–188 (2005)

[7] Alves, C.J.S., Chen, C.S.: A new method of fundamental solutions applied to non-homogeneous elliptic problem. Advances in Computational Mathematics **23**(1), 125–142 (2005)

[8] Jones, R.S.: Computing ultra-precise eigenvalues of the Laplacian within polygons. Adv. Comput. Math **43**(6), 1325–1354 (2017)

[9] Fletcher, C.A.J.: Computational Galerkin Methods. Scientific Computation. Springer, New York (1984)

[10] Lebedev, V.I.: Values of the nodes and weights of quadrature formulas of gauss–markov type for a sphere from the ninth to seventeenth order of accuracy that are invariant with respect to an octahedron group with inversion. U.S.S.R. Comput. Math. Math. Phys. **15**, 44–51 (1975)

[11] Lebedev, V.I.: Spherical quadrature formulas exact to orders 25–29. Sib. Math J. **18**, 99–107 (1977)

[12] Betcke, T., Trefethen, L.N.: Reviving the method of particular solutions. SIAM J. Numer. Anal. **47**(3), 469–491 (2005)

[13] Golub, G.H., Van Loan, C.F.: Matrix Computations, 4th edn. Johns Hopkins University Press, Baltimore, MD (2013)

[14] Barnett, A.H.: Perturbative analysis of the method of particular solutions for improved nclusion of high-lying dirichlet eigenvalues. SIAM J. Numer. Anal. **47**(3), 1952–1970 (2009)

[15] Moler, C.B., Payne, L.E.: Bounds for eigenvalues and eigenvectors of symmetric operators. SIAM J. Numer. Anal. **5**, 64–70 (1968)

[16] Kato, T.: Perturbation Theory for Linear Operators, 2nd edn. Springer, Berlin, Heidelberg (1995)

[17] Dahlen, F.A.: The Normal Modes of a Rotating, Elliptical Earth. Geophys. J. R. Astr. SOC **16**, 329–367 (1968)

[18] Troesch, B.A., Troesch, H.R.: Eigenfrequencies of an Elliptic Membrane. Mathematics of Computation **27**, 755–765 (1973)

[19] Jones, R.S.: The fundamental Laplacian eigenvalue of the ellipse with Dirichlet boundary conditions (2018). https://arxiv.org/abs/1802.07768

[20] Grebenkov, D.S., Nguyen, B.-T.: Geometrical structure of Laplacian eigenfunctions. SIAM Review **55**(4), 601–667 (2013)

[21] Sapoval, B., Haeberlé, O., Russ, S.: Acoustical properties of irregular and fractal cavities. The Journal of the Acoustical Society of America **102**(4), 2014–2019 (1997)